What Tunes the Structural Anisotropy of Magnetic Fluids under a Magnetic Field?

ARTICLE *in* THE JOURNAL OF PHYSICAL CHEMISTRY B · APRIL 2006

Impact Factor: 3.3 · DOI: 10.1021/jp0558573 · Source: PubMed

7 AUTHORS, INCLUDING:

François Boué
French National Centre for Scientific Research
211 PUBLICATIONS **4,454** CITATIONS
SEE PROFILE

Andrejs Cebers
University of Latvia
156 PUBLICATIONS **1,586** CITATIONS
SEE PROFILE

What Tunes the Structural Anisotropy of Magnetic Fluids under a Magnetic Field?

Guillaume Mériguet,[†] Fabrice Cousin,[†,‡] Emmanuelle Dubois,[*,†] François Boué,[‡] Andrejs Cebers,[§] Bela Farago,[||] and Régine Perzynski[†]

Laboratoire Liquides Ioniques et Interfaces Chargées, UPMC, UMR CNRS-UPMC-ESPCI 7612, case 51, 4 place Jussieu, 75252 Paris Cedex 05, France, Laboratoire Léon Brillouin, CEA CNRS UMR 12, CE Saclay, 91191 Gif-sur-Yvette, France, Latvian Academy of Sciences, Institute of Physics, LV-2169 Salaspils, Latvia, and Institut Laue Langevin, BP 156, 38042 Grenoble, France

Received: October 13, 2005; In Final Form: January 2, 2006

In the present study, the structure of monophasic ionic magnetic fluids under a static magnetic field is explored. In these aqueous electrostatically stabilized ferrofluids, we vary both the isotropic interparticle interactions and the anisotropic dipolar magnetic interaction by tuning the ionic strength and the size of the nanoparticles. Small angle neutron scattering measurements carried out on nanoparticles dispersed in light water exhibit miscellaneous 2D nuclear patterns under a magnetic field with various q-dependent anisotropies. In this nondeuterated solvent where the magnetic scattering is negligible, this anisotropy originates from an anisotropy of the structure of the dispersions. Both the low q region and the peak of the structure factor can be anisotropic. On the scale of the interparticle distance, the structure is better defined in the direction perpendicular to the field. In the thermodynamic limit ($q \rightarrow 0$), the model previously described in ref 10 matches the data without any fitting parameters: the interparticle interaction is more repulsive in the direction parallel to the magnetic field. At low q, the amplitude of the anisotropy of the pattern is governed by the ratio of two interaction parameters: the reduced parameter of the anisotropic magnetic dipolar interaction, γ/Φ, over the isotropic interaction parameter, K_T°, in zero field, which is proportional to the second virial coefficient.

I. Introduction

The magnetic fluids (MFs) studied here are colloidal dispersions of magnetic nanoparticles, which can be, due to their magnetic properties, used in numerous applications, like seals, sensors, or loudspeakers.[1,2] Their properties without and with a magnetic field, for example, the viscosity or the magnetic susceptibility, are strongly affected by the microstructure of the dispersions.[2] Several studies deal with the microstructure of ferrofluids under a magnetic field; however, no general behavior is clear at this stage.[3−18] This may result from the diversity of behaviors already observed in MFs without a magnetic field. The aim of this paper is to explore a well-defined subset of possible behaviors, which we wish to define now.

First, let us emphasize that the nanocolloidal systems considered clearly differ from magnetorheological suspensions (MRS). MRS are constituted of much bigger particles which have no dipolar moment in zero magnetic field. The dipolar moment is induced under field and can reach high values, easily allowing the formation of chainlike structures, which strongly modify the properties of the suspensions, thus used for several kinds of applications such as clutches and dampers.[19] On the contrary, in magnetic fluids, each nanoparticle has a dipole moment independent of the value of a magnetic field.

Even in the more restricted case of nanoparticles, ferrofluids still present various situations, as first observed in the absence of a field. Numerous studies reveal larger objects, controlled by several parameters. The existence of chains is one of the most debated topics in MFs; recently, in monodisperse systems, chains have been observed above a given magnetic moment, μ, of the nanoparticles, leading to a high enough magnetic dipolar interaction.[11,12] A large enough μ is obtained above a characteristic size (which depends on the material). Therefore, in polydisperse systems, the formation of chains is favored by the presence of big particles.[7,13,20] If the magnetic dipolar interaction is not high enough to favor chains, aggregates can nevertheless exist as well as isolated nanoparticles, and this is controlled by the other interactions, both repulsive and attractive,[13−17] which are crucial.

Under a magnetic field, the particles, clusters, or chains tend to orientate along the field direction in rather small fields, for example, about 800 kA/m (10 kOe) for the full orientation of ferrite nanoparticles (diameter around 10 nm). Besides this individual effect of orientation, cooperative behavior may arise for a large concentration of nanoparticles, since the balance of interparticle interactions is modified. For certain cases, the result of these interactions is that the suspensions may separate into two phases,[2,21−29] one poor in nanoparticles and a rich one (20−30% vol/vol) organized as micronic needles parallel to the field. Finally, even if the suspension remains monophasic, various situations are seen using scattering techniques (small angle neutron (or X-ray) scattering, SANS (SAXS)), well adapted to the investigation of such systems. Depending on the magnetic fluid used, no anisotropy is observed on the structure factor,[4] chains are observed,[5−7] field induced organizations occur,[8] or a structural anisotropy on a spatial scale of the interparticle distance is reported.[9,10]

The subset on which we focus here includes only monophasic samples in which no chains are present without a magnetic field (μ small enough), under well controlled and characterized conditions. For this purpose, our great allies are chemistry and

* Corresponding author. Phone: 33 1 44 27 32 67. Fax: 33 1 44 27 32 28. E-mail: emdubois@ccr.jussieu.fr.
[†] UPMC, UMR CNRS-UPMC-ESPCI 7612.
[‡] CEA CNRS UMR 12.
[§] Institute of Physics.
[||] Institut Laue Langevin.

10.1021/jp0558573 CCC: $33.50
Published on Web 02/11/2006

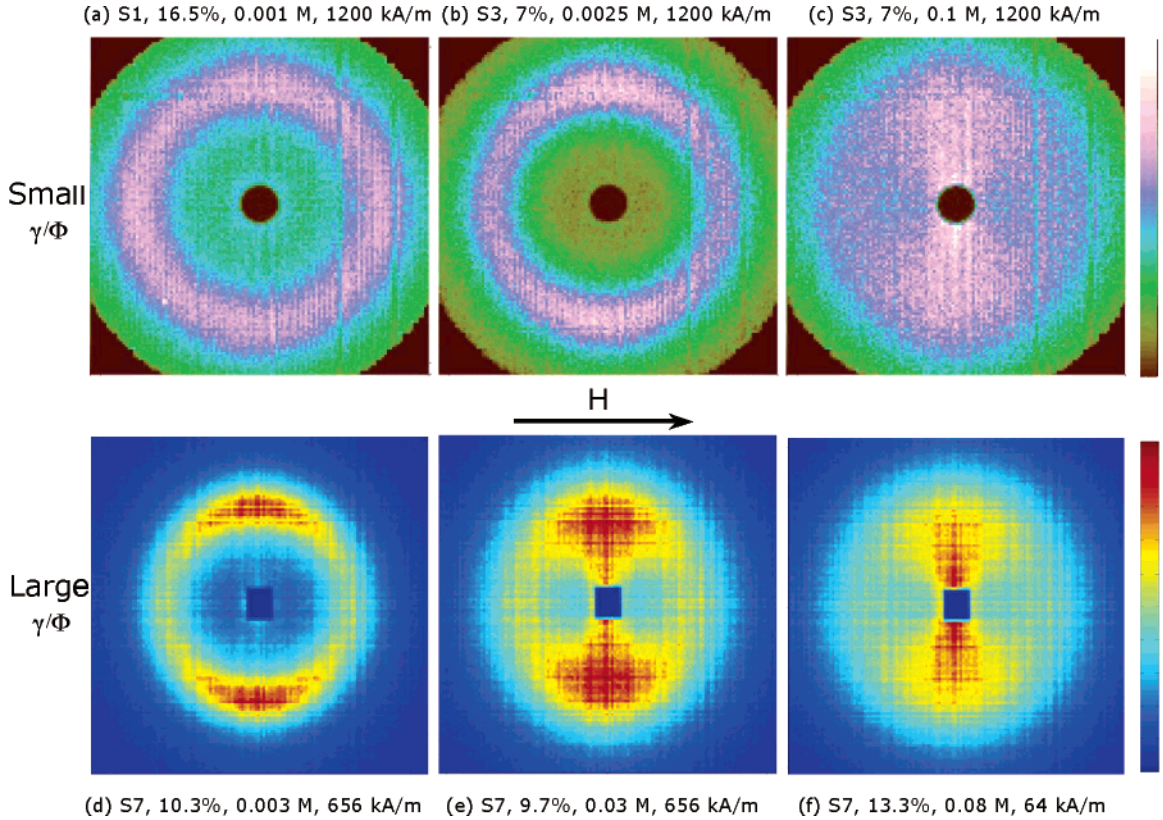

Figure 1. Raw spectra of the scattered intensity by the maghemite dispersions on the 2D detector. A magnetic field is applied in the horizontal direction. The intensity increases from the bottom to the top of the color scale given on the right. The ionic strength is increasing from left to right. The top row corresponds to small particles (small dipole moment, μ, and small magnetic dipolar parameter, γ/Φ), and the bottom row corresponds to big particles (large μ, large γ/Φ). For each pattern, the experimental features are given in the following order: nanoparticles (see Table 1), volume fraction, $[\text{citrate}]_{\text{free}}$, magnetic field. These patterns correspond to fluid samples except for part a which corresponds to a solid sample.

physicochemistry. We synthesize aqueous ferrofluids ourselves, that we have extensively studied without a field. Controlling the size and the surface of the nanoparticles as well as the composition of the solution yields a wide accessible range for the ratio of isotropic repulsive interactions over the attractive interactions. Also, the osmotic pressure of these aqueous dispersions can be strongly varied. It allows a much wider exploration of the phase diagram osmotic pressure, Π/volume fraction, Φ, of the dispersions (equivalent to the $P-V$ diagram for atomic systems), as described in ref 30. This is at variance with oily ferrofluids, that is, surfacted particles in organic solvents; for moderate osmotic pressures, the two systems are however very similar in their interparticle interactions and properties.[31] We want here to explore the large fluid area of the phase diagram[30] in the presence of a field; this is an extension of our previous work,[10] dedicated to such aqueous systems, under field, at moderate osmotic pressures, corresponding to a weak repulsion.

Inside this wide fluid phase area, the SANS pattern anisotropy is very diverse, as illustrated in Figure 1: no anisotropy at all (a), anisotropy at an intermediate spatial scale (b and d) or anisotropy at all of the probed spatial scales (c, e, and f). We will see below that the knowledge of the behavior without a field is *essential* for understanding the behavior under a field, because isotropic dipolar interactions compete for control of the amplitude and the spatial scale of the anisotropy.

II. Colloidal Magnetic Suspensions

The systems studied are dispersions of maghemite (γ-Fe_2O_3) nanoparticles in water. The particles are chemically synthesized[31,32] and then coated with citrate molecules, which ensure a negative charge at neutral pH. At the end of the synthesis, the diameters of the particles are polydisperse with a mean around 7 nm. The polydispersity can be reduced using a routine size-sorting procedure based on the properties of the phase transitions induced by an increase of ionic strength.[24] The size distribution is described by a log-normal law,[2] determined by two parameters: the diameter, d_0 ($\ln d_0 = \langle \ln d \rangle$), and the polydispersity index, σ (σ is the standard deviation of $\ln d$). It varies from 0.35 before size sorting down to 0.15−0.2 after the size sorting.

In these dispersions, the surface charge is 2 e^-/nm^2,[31] the particles are dispersed in water at pH 7.5, and the ionic strength is due to the free sodium citrate concentration, $[\text{citrate}]_{\text{free}}$, which has to be high enough ($>2 \times 10^{-3}$ mol/L) in order to ensure the maximal charge of 2 e^-/nm^2. Note that, if $[\text{citrate}]_{\text{free}}$ is lower than 2×10^{-3} mol/L, the charge of the particle decreases (at first order decreasing the repulsion intensity); however, the ionic strength also decreases (which enhances the repulsion range). Balancing those two parameters, we obtain, down to $[\text{citrate}]_{\text{free}} = 10^{-3}$ mol/L,[33] dispersions which are indeed stabilized by electrostatic repulsion. Without a magnetic field, for nanoparticles of a given size, and at a given temperature (here $T = 300$ K), their dispersions are fully characterized by two parameters among the three following ones: the *osmotic pressure*, Π, the *volume fraction*, Φ, *and the ionic strength*, I (fixed by $[\text{citrate}]_{\text{free}}$ here). The osmotic pressure can be measured for low pressures (<4000 Pa). For larger pressures, it is imposed, using the osmotic compression method,[34] which allows us to explore wide regions of the phase diagram. The solution is placed in a dialysis bag that is put in a bath containing sodium citrate, which controls the ionic strength, I, and polymer (dextran $M_w = 1.1 \times 10^5$

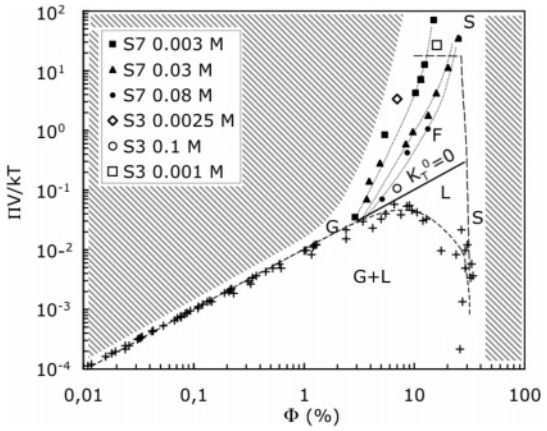

Figure 2. Phase diagram of our dispersions obtained from previous work.[30] G = gas, L = liquid, F = fluid, S = solid, the hatched regions cannot be reached, and the crosses are experimental data on the coexistence line between the gas and the liquid. The dashed lines are guides for the eye for the coexistence line between the gas and the liquid, and the limit between fluids and solids. The full straight line corresponds to a second virial coefficient equal to zero. Data for small particles (S3, $\gamma/\Phi = 12$) and big particles (S7, $\gamma/\Phi = 34$) are plotted in the graph. The lines through the points in the fluid area are guides for the eye corresponding to series of same ionic strength for sample S7. The correspondence between symbols and dispersions is given in the legend (nanoparticle S3 or S7, $[\text{citrate}]_{\text{free}}$).

g/mol, Fluka), which controls the osmotic pressure, Π. As the equilibrium of the pressures inside and outside the bag takes a long time to reach, we wait for 3 weeks to be sure we are at equilibrium. Then, Π and I are fixed, and we only measure Φ by chemical titration of iron.[35] Controlling and varying the three parameters—pressure, Π, volume fraction, Φ, and $[\text{citrate}]_{\text{free}}$—has allowed us to build up the phase diagram of the system which is presented in ref 30 (see Figure 2). This phase diagram is similar to the one of atomic systems: gas, liquid, fluid, and solid phases can be observed. The plotted ordinate is the ratio $\Pi V/kT$, with V being the volume of the nanoparticles, to renormalize the influence of the mean size of the particle (Π is proportional to $1/V$ at first order). In this diagram, a high ionic strength, which decreases the interparticle repulsion, gives a lower equilibrium pressure, Π, at a given Φ value, which corresponds to lower values of $\Pi V/kT$. In the present study, we analyze the structure under a magnetic field of dispersions constituted of nanoparticles of various sizes in the monophasic regions of this diagram (fluid or solid). Let us recall that all of the samples studied in our previous investigations under a field[10,36] were weakly repulsive fluids located in the fluid area at a moderate osmotic pressure of the phase diagram (see Figure 2). They were not prepared using the technique of osmotic compression. Here, this technique allows us to explore wider regions of the phase diagram and more various behaviors, because the control parameters Π, Φ, and $[\text{citrate}]_{\text{free}}$ can be varied in a large range.

To characterize the magnetic interaction, we must introduce the ratio, γ, of magnetic dipolar potential over kT:

$$\gamma = \frac{\mu_0 \mu^2}{\bar{r}^3 kT} = \frac{\mu_0 m_s^2 \pi d^3}{6kt}\Phi \qquad (1)$$

where $\mu = m_s \pi d^3/6$ is the magnetic moment of the nanoparticles ($\mu \sim 10^4$ Bohr magnetons), m_s is the magnetization of the material (here $m_s = 3.1 \times 10^5$ A/m), and $\bar{r}$ is the mean interparticle distance. The ratio γ/Φ corresponds to the potential between two orientated dipoles at contact. Therefore, it only depends on m_s and d (at a given temperature, T) and is independent of Φ. For an easier comparison with the literature, we shall also give the reduced parameter, $\lambda^* = \mu_0 \mu^2/(4\pi d^3 kT)$, linked to γ/Φ by $\lambda^* = (\gamma/\Phi)/24$.

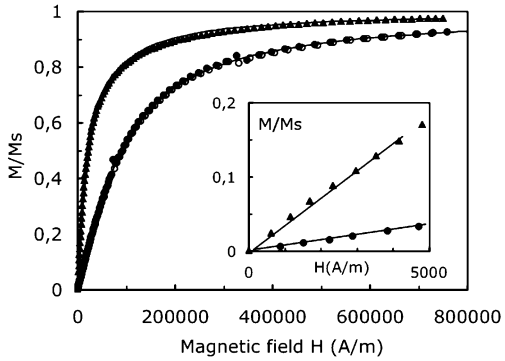

Figure 3. Experimental magnetization curve (symbols) of dilute dispersions (Φ < 1%) and fit with Langevin's law and a log-normal polydispersity (lines). The inset plots the data at low magnetic field, where the variation is linear with H, with the slope being the magnetic susceptibility, proportional to γ/Φ. Dots: nanoparticle S1, $d_0 = 6.8$ nm, $\sigma = 0.16$, and $\gamma/\Phi = 7$, $\lambda^* = 0.29$. Triangles: nanoparticle S7, $d_0 = 9$ nm, $\sigma = 0.28$, $\gamma/\Phi = 34$, $\lambda^* = 1.42$.

TABLE 1: Characteristics of the Ferrofluids Used[a]

name	d_0	σ	γ/Φ	λ^*
S1	6.8	0.16	7	0.29
S2	7.1	0.15	9	0.37
S3	7.3	0.22	12	0.5
S4	8.5	0.15	14	0.58
S5	9.5	0.2	24	1
S6	8.9	0.3	25	1.04
S7	9.8	0.25	34	1.42

[a] d_0 and σ, characteristics of the magnetic size distributions of the ferrofluids; γ/Φ or λ^*, value of the reduced dipolar interaction parameter.

If the dispersion is dilute enough ($\gamma \leq 1$), an applied magnetic field, H, only orientates the magnetic moment of the γ-Fe_2O_3 particles. Figure 3 shows typical magnetization curves, $M = f(H)$, for dilute solutions: the particles are fully orientated around 800 kA/m (10 kOe). For monodisperse particles, one expects Langevin's law: $M = m_s \Phi L(\xi)$, where $\xi = \mu_0 \mu H/kt$ is the Langevin parameter and $L(\xi) = \coth \xi - 1/\xi$ is the Langevin function. For polydisperse particles, this Langevin function has to be weighted by the log-normal distribution of the diameters of the nanoparticles.[2] The fit of the data (see Figure 3) then allows a determination of d_0 and σ, listed in Table 1. The difference of orientation between small and large particles for a fixed applied field is clearly visible in Figure 3. The parameter γ/Φ is determined from the initial susceptibility, χ_0, which equals $\gamma/3$ at low Φ (see the inset of Figure 3 and values in Table 1).

At large volume fractions, the magnetic dipolar interaction becomes significant. Provided that the solution remains monophasic under a field, an effective field formalism may be used to model the magnetization of the dispersion. It is $M = m_s \Phi L(\xi_e)$, where the effective Langevin parameter, ξ_e, is given by $\xi_e = \xi + \lambda \gamma L(\xi_e)$, with λ being the effective field constant.[37] In our MF system, this effective field constant has been found to be equal to 0.22,[10,36,38] a value lower than the classical Lorentz value 0.33,[39] also reproduced by numerical simulations.[40]

Applying a field is, from a mean-field point of view, equivalent to increasing the interparticle attractions. Like for an increase of ionic strength, it corresponds to a vertical fall in

the $\Pi-\Phi$ diagram. This can induce a phase separation if the pressure before applying a field is already close to the coexistence line. For such systems with a low pressure (close to the coexistence line of the gas−liquid transition), the occurrence or not of a phase separation under a magnetic field is not a priori obvious. The stability has to be checked experimentally, to be sure to study monophasic samples. In practice, three steps are taken: (i) the stability without a field is checked for all of the samples using optical microscopy observations, and the citrate concentration value inducing a phase separation without a field is measured (the threshold is, for example, 0.4 mol/L for sample S3 or S1); (ii) then, the maximal $[\text{citrate}]_{\text{free}}$ values used in the samples are kept low enough in order to avoid phase separation under a magnetic field; (iii) this is checked experimentally up to fields as high as 15 000 Oe (1200 kA/m) using a laser beam that passes through the sample while the field is applied. If two phases are present under a field, one phase forms long needles elongated along the field and a strong diffraction line is observed in the direction perpendicular to the field.[23] We never observe such diffraction patterns with our samples with the values of magnetic fields used. In practice here, a maximum of $[\text{citrate}]_{\text{free}} = 0.1$ mol/L has been used with sample S3 (H up to 1200 kA/m), and this value is 0.08 mol/L with sample S7 (H limited to 120 kA/m).

III. Small Angle Neutron Scattering: Measurements and Modeling at Low q

III.1. Measurements. The SANS intensity scattered by our samples can be separated into two contributions: the nuclear scattering, I_N, and the magnetic scattering, I_M. I_N can be tuned by contrast variation, not I_M. I_N is maximum in light water and decreases while increasing the proportion of heavy water. This results in the fact that, in H_2O, $I_N \gg I_M$ according to estimated calculations, whereas this is no longer true in D_2O. This has been confirmed experimentally by polarization analysis of scattered intensities.[36] Therefore, we prepare all samples in H_2O and neglect magnetic scattering; in practice, what we measure here is nuclear scattering, I_N, called $I(q)$ from now on for simplification.

The SANS experiments have been performed on PAXY for samples S3 and S1 (reactor Orphée, LLB, CEA-Saclay, France). Two configurations have been used: a wavelength of $\lambda = 5$ or 10 Å and a distance between the sample and the detector of $D = 3.1$ m. With an applied field, the scattered intensity has been measured only in the configuration ($\lambda = 5$, $D = 3.1$ m) which allows measuring the peak in the structure factor. For sample S7, SANS experiments have been performed on D22 (ILL, Grenoble, France). Two configurations have been used: $\lambda = 7$ Å and a distance between the sample and the detector of $D =$ 2 and 8 m. With both spectrometers, the intensity is recorded on a two-dimensional detector. Without a field, the intensity is averaged over a circle, leading to $I(q)$. Under a field, the intensity is averaged on sectors with a width of 20°. Here, we mainly present the results along the directions parallel ($I_{\parallel}(q)$) and perpendicular ($I_{\perp}(q)$) to the magnetic field, associated to the stronger variations. The intensity is then treated in order to subtract the scattering from the solvent and the quartz cell.

Considering the nanoparticles are roughly spherical, $I(q)$ can be written as $I(q)\ (\text{cm}^{-1}) = \Phi V_w \Delta\rho^2 F(q) S(q)$, where V_w is the weight averaged volume of the scattering objects, $\Delta\rho^2$ is the contrast between the particles and the solvent, $F(q)$ is the form factor, and $S(q)$ is the structure factor. The form factor, with a Guinier plateau at low q, is determined experimentally from dilute suspensions in which the interparticle interactions are negligible ($S(q) \sim 1$), typically with $\Phi_d < 1\%$ and $[\text{citrate}]_{\text{free}} = 0.03$ M. It then allows us to determine experimentally the structure factor of concentrated suspensions of volume fraction, Φ_c, by $S(q) = (I(q, \Phi_c)/\Phi_c)/(I(q, \Phi_d)/\Phi_d)$.

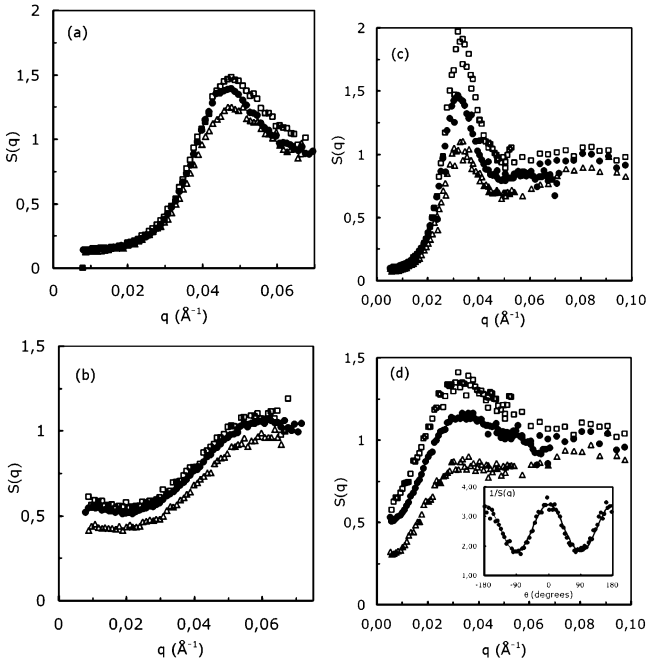

Figure 4. Structure factors for samples S3 (a and b, $\gamma/\Phi = 12$) and S7 (c and d, $\gamma/\Phi = 34$) without a field (full circles), parallel to the field (triangles), and perpendicular to the field (squares): (a) nanoparticle S3, $\Phi = 7\%$, $[\text{citrate}]_{\text{free}} = 0.0025$ M, $H = 15\,000$ Oe (raw data: Figure 1b); (b) nanoparticle S3, $\Phi = 7\%$, $[\text{citrate}]_{\text{free}} = 0.1$ M, $H =$ 15 000 Oe (raw data: Figure 1c); (c) nanoparticle S7, $\Phi = 10.3\%$, $[\text{citrate}]_{\text{free}} = 0.003$ M, $H = 8200$ Oe (raw data: Figure 1d); (d) nanoparticle S7, $\Phi = 4.9\%$, $[\text{citrate}]_{\text{free}} = 0.03$ M, $H = 8200$ Oe (raw data similar to Figure 1f). The inset in Figure 4d plots $1/S(q)$ as a function of the angle, θ, between q and H for $q = 0.0085$ Å^{-1}.

A measurement with $H = 0$ is performed for each sample before and after measurements under a field in order to check the reversibility of the observed phenomena. For all samples, the observed anisotropy appears as perfectly reversible, since it disappears when the field is suppressed.

The results are the following:

(1) Without a field, $I(q)$ always remains isotropic.

(2) Under a field, for all of the dilute samples (with negligible magnetic dipolar interaction, $\gamma \leq 1$), no anisotropy has been observed. Therefore, an anisotropy only due to the form factor of isolated particles is excluded.

(3) Under a field, for concentrated samples, *the observation of anisotropy is not systematic*. However, when an anisotropy is observed, we can assert that it corresponds to an anisotropy of the structure factor only, since it can be due neither to the form factor, as seen above for dilute particles, nor to magnetic scattering, which is negligible in light water.

Figure 4 compares the isotropic structure factor, $S(q)$, obtained at $H = 0$ to the corresponding structure factors under a field, $S_{\parallel}(q) = I_{\parallel}(q)/P(q)$ and $S_{\perp}(q) = I_{\perp}(q)/P(q)$, for four samples corresponding to the different families of 2D patterns of Figure 1. In the next sections, a quantitative analysis of these structure factors at low q is presented both without and with an applied magnetic field.

III.2. Analysis of the Behavior at Low q in Zero Field. In the $q = 0$ limit, the scattered intensity is proportional to the

TABLE 2: Characteristics of Some Dispersions Based on Nanoparticles S1, S3, and S7[a]

sample	[citrate] (mol/L)	phase	K_T°	Φ	γ/Φ	Ani_{max}
S1	0.001	S	>100	0.165	7	<0.1
S3	0.0025	F	106	0.07	12	0.1
S3	0.1	F	11.7	0.07	12	0.9
S7	0.003	F	72; 79; >100	0.029; 0.05; 0.103	35	0.35
S7	0.03	F	17; 43	0.037; 0.097	35	1.14
S7	0.08	F	25	0.133	35	2.1

[a] Phase: S = solid, F = fluid. K_T°, second virial coefficient as defined by eq 3; Φ, volume fraction of the nanoparticles; γ/Φ, reduced magnetic dipolar parameter; Ani_{max}, value of the anisotropy of interaction at high field, as defined by eq 8.

osmotic compressibility, χ_T, of the suspension:

$$\left(\frac{\Phi}{I}\right)_{q=0} = \frac{1}{V_w\Delta\rho^2}\frac{\partial}{\partial\Phi}\left(\frac{\Pi V_w}{kT}\right) = \frac{1}{V_w\Delta\rho^2}\frac{1}{\chi_T} = \frac{1}{V_w\Delta\rho^2}S^{-1}(q=0,\Phi) \quad (2)$$

It can then be written as the following first-order expression in Φ:

$$\left(\frac{\Phi}{I}\right)_{q=0} \approx \frac{1}{V_w\Delta\rho^2}(1 + K_T^\circ\Phi) \quad (3)$$

In this formula, K_T° is a dimensionless parameter, which is proportional to the second virial coefficient. It takes into account all of the interparticle interactions (hard core repulsion, van der Waals attraction, electrostatic repulsion, dipolar interaction). In practice, we know that a linear variation of Φ/I with Φ is observed up to high volume fractions (around 20%), as reported in ref 10 (Figure 4 in ref 10). Table 2 lists K_T° for several sizes of nanoparticles, ionic strengths, and volume fractions. In the dispersions studied here, K_T° is positive, which means the global interparticle interactions always remain repulsive in these dispersions. As a result, there is no particle aggregation, no correlation domains associated to the fluctuation of concentration, but individual fluctuations of position of the particles.[10]

III.3. Modeling of the Low *q* Behavior under an Applied Magnetic Field. Under a magnetic field, H, the compressibility of the system becomes anisotropic and K_T° transforms in $K_T(H, \theta)$ where θ is the angle between the field and the scattering vector, q. Indeed $K_T^\circ = K_T(H=0, \theta)$ and is independent of θ. A model based on a low q expansion of the free energy under an applied field has been previously developed in refs 10 and 38. This effective field model leads to the following expression for the value of $K_T(H,\theta)$:

$$K_T(H,\theta) = K_T^\circ - \left(\frac{\alpha_\lambda(H)}{\Phi}\right) + \left(\frac{\beta_\lambda(H)\cos^2\theta}{\Phi}\right) \quad (4)$$

with

$$\alpha_\lambda(H) = \lambda\gamma\frac{L^2(\xi_e)}{(1 - \lambda\gamma L'(\xi_e))} \quad (5)$$

and

$$\beta_\lambda(H) = \frac{\gamma L^2(\xi_e)}{[1 - \lambda\gamma L'(\xi_e)][1 + (1-\lambda)\gamma L'(\xi_e)]} \quad (6)$$

K_T is the sum of three terms:

(1) The first one, K_T°, is the isotropic contribution independent of H described in section III.2.

(2) The second one, $-\alpha_\lambda/\Phi$, is an isotropic and attractive mean-field contribution, which accounts for the short range aspect of dipolar interactions, aforementioned in section II.

(3) The third one, $\beta_\lambda \cos^2\theta/\Phi$, is an anisotropic and repulsive contribution; it is maximum in the direction parallel to the field and equals zero in the direction perpendicular to the field; this contribution accounts for the long range effect of the dipolar magnetic interaction and is related to the anisotropic fluctuations of a macroscopic field, and thus to demagnetizing effects. The system tends to flatten the heterogeneities of a magnetic field in this direction.

Consequently, K_T° depends on the field amplitude and tends toward $K_T(H,\theta) = K_T^\circ - (\lambda\gamma/\Phi) + ((\gamma/\Phi)\cos^2\theta)$ for high fields. As λ is smaller than 1, $K_T^{||} > K_T^\circ$ and the repulsion is stronger in the parallel direction than at $H = 0$, while $K_T^\perp < K_T^\circ$ and the repulsion is weaker in the perpendicular direction than at $H = 0$. This result is nonintuitive because one would expect attractions and the formation of chains in the parallel direction, as in magnetorheological suspensions (MRS). However, chains can be formed only for high values of λ^*. If, for MRS, λ^* increases with the magnetic field (as explained in the Introduction), leading to chains by increasing the magnetic field, on the contrary, in our MF systems, the size of the particles and the nature of the used material set the value of λ^*, which is small enough to preclude the formation of chains. This has been concluded from our previous experiments and is in good agreement with numerical simulations of our system at $\gamma/\Phi = 34$ ($\lambda^* = 1.42$)[41] and also simulations of different ferrofluids varying λ^* from 1 to 8,[42] which show no formation of chains for small values of λ^* as in our system.

IV. Analysis of the Pattern Anisotropy at Low *q*

Several parameters influence the SANS patterns at low q, namely, the volume fraction, Φ, of the dispersion, the reduced dipolar parameter, γ/Φ (or λ^*), of the nanoparticles, the interaction parameter, K_T°, and the strength of H if a magnetic field is applied.

In practice here, the dipolar parameter, γ/Φ, only depends on the size of the nanoparticles. The interaction parameter, K_T°, however depends on all of the interparticle interactions, that is, on the repulsion, which is controlled by $[citrate]_{free}$, and on the dipolar part of the attraction, which is controlled by γ/Φ. Quantitatively, K_T° is tuned by $[citrate]_{free}$ in the range of accessible parameters, here $[citrate]_{free} > 0.001$ M, and by $\gamma/\Phi < 40$ ($\lambda^* < 1.65$).

To sort out the respective influences of the four parameters H, Φ, γ/Φ, and K_T°, let us first analyze the anisotropy of the compressibility under an applied field, before returning to the patterns and to the anisotropy of scattered intensity.

A. Anisotropy of the Interactions. In the framework of our model, using eqs 4−6, the under-field anisotropy of interactions is completely described by the anisotropy of the second virial coefficient, K_T, which is directly linked to the anisotropy of the compressibility (see eq 3). Therefore, $S^{-1}(q=0,\Phi)$ varies as $\cos^2\theta$, with θ being the angle between q and H. An example is plotted as an inset in Figure 4d. Focusing on the two directions $\theta = 0$ (||) and $\theta = \pi/2$ ($\perp$), the anisotropy of K_T is quantified

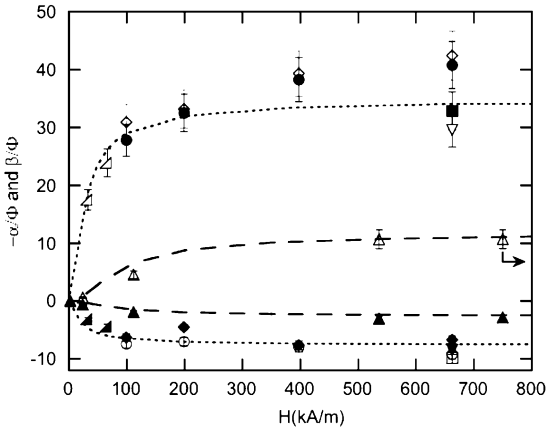

Figure 5. β_λ/Φ and $-\alpha_\lambda/\Phi$ plotted versus H for nanoparticles S3 and S7, varying ionic strength and volume fraction. The lines correspond to the model described in the text (no fitting parameters). The dots are the experimental data: for each sample, the same shape of symbol is used for β_λ/Φ and $-\alpha_\lambda/\Phi$; however, the symbol is open or full. The curves of β_λ/Φ are the positive ones, and the curves of $-\alpha_\lambda/\Phi$ are the negative ones. Nanoparticle S3: (triangles) $[\text{citrate}]_{\text{free}} = 0.1$ mol/L. The triangle plotted at 750 kA/m should appear out of the scale, at 1228 kA/m. Nanoparticle S7: (half squares) $\Phi = 13.3\%$, $[\text{citrate}]_{\text{free}} = 0.08$ M; (inverse triangles) $\Phi = 2.9\%$, $[\text{citrate}]_{\text{free}} = 0.003$ M; (squares) $\Phi = 5\%$, $[\text{citrate}]_{\text{free}} = 0.003$ M; (circles) $\Phi = 3.7\%$, $[\text{citrate}]_{\text{free}} = 0.03$ M; (diamonds) $\Phi = 9.7\%$, $[\text{citrate}]_{\text{free}} = 0.03$ M.

by the two functions α_λ/Φ and β_λ/Φ:

$$K_T^\perp - K_T^\circ = -\alpha_\lambda/\Phi$$

$$K_T^{||} - K_T^\perp = \beta_\lambda/\Phi \tag{7}$$

These functions α_λ/Φ and β_λ/Φ do not depend on the global average interparticle interaction quantified by K_T°. Consequently, they neither depend on the osmotic pressure, Π, nor depend on the location of the dispersion in the phase diagram in zero field (Figure 2). Moreover, in our range of parameters, and within a precision of the order of 1%, we expect that they do not depend on Φ. The unique control parameters of α_λ/Φ and β_λ/Φ are thus H and γ/Φ.

The experimental evolutions of $K_T^\perp - K_T^\circ$ and $K_T^{||} - K_T^\perp$ are plotted as a function of H in Figure 5 for two values of γ/Φ (small and large particles), as well as the calculated values of α_λ/Φ and β_λ/Φ. Note that they are calculated with the experimental values of γ/Φ, H, μ, Φ, and $\lambda = 0.22$, as in ref 38. There is no new adjusted parameter. Therefore, Figure 5 shows that the experimental variation of the anisotropy of interaction as a function of the magnetic field is well described by the model. Moreover, as expected, there is influence neither of the volume fraction, Φ, nor of the mean global interaction, K_T°. On the contrary, it shows the drastic influence of the parameter γ/Φ.

Figure 6 validates our model: it displays the entire set of results as $(K_T^{||} - K_T^\perp)_{\text{experimental}}$ plotted as a function of the theoretical values β_λ/Φ, calculated using the experimental values of the parameters γ/Φ, H, μ, Φ, and $\lambda = 0.22$. In Figure 6, we have added results obtained in ref 36 with samples of various γ/Φ (samples S2, S4, S5, and S6, see Table 1). The linear correlation is rather good. With our model, the anisotropy of the second virial coefficient is thus correctly predicted whatever the magnetic field and the sample for $7 \leq \gamma/\Phi \leq 35$, $0 \leq \Phi \leq 16.5\%$, and $16 \leq K_T^\circ \leq 100$.

B. Anisotropy of the Scattered Intensity. If we go back to the patterns of Figure 1, focusing on the low q behavior, it

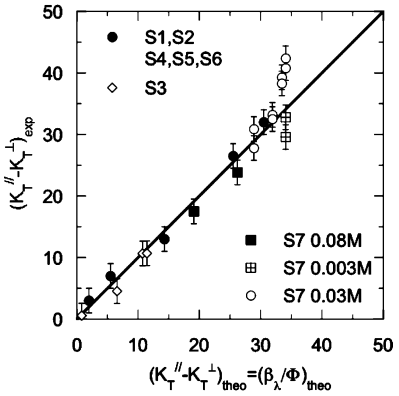

Figure 6. Anisotropy of K_T measured versus the expected one as obtained from eqs 6 and 7 for particles of different sizes: (full circles) $H = 68$ kA/m (850 Oe), γ/Φ varies from 9 to 42, nanoparticles S1, S2, S4, S5, and S6;[36] (open diamonds) nanoparticle S3 ($\gamma/\Phi = 12$) for several values of the magnetic field (data of Figure 5); (other data) nanoparticle S7 ($\gamma/\Phi = 34$) plotted for the three ionic strengths and various magnetic fields, H (data of Figure 5).

appears that in some situations there is no detectable anisotropy (Figure 1a), although $K_T^{||} - K_T^\perp$ is constant whatever the location of the dispersion in the $\Pi-\Phi$ diagram in zero field (Figure 2). In fact, the anisotropy of scattered intensity is not only sensitive to the anisotropic part of the interparticle interaction, but it is also sensitive to its isotropic part.

Indeed, the relative anisotropy of interactions can be quantified by eq 8:

$$\text{Ani} = \frac{K_T^{||} - K_T^\perp}{K_T^\circ} = \frac{\dfrac{\beta_\lambda}{\Phi}}{K_T^\circ} \tag{8}$$

which tends toward $\text{Ani}_{\text{max}} = (\gamma/\Phi)/K_T^\circ$ in high fields. It is the ratio of the reduced dipolar interaction parameter, γ/Φ, responsible here for the anisotropic part of the interparticle interaction over the parameter K_T°, characteristic of the total interaction in zero field. The values of Ani_{max} for all of our samples are reported in Table 2. It varies here between 0.1, typically obtained with large $K_T^\circ \sim 100$ and low $\gamma/\Phi \sim 10$ ($\lambda^* \sim 0.4$), up to values larger than 1 for $K_T^\circ < \gamma/\Phi$.

The anisotropy at low q of the scattered intensity, seen from the patterns in Figure 1, can be quantified by $\Delta I/I_{\text{mean}} = 2(I_\perp - I_{||})/(I_\perp + I_{||})$. Experimentally, this anisotropy of scattered intensity can be detected only if it is larger than the error of $I(q)$. In high fields, $\Delta I/I_{\text{mean}}$ is maximum and its value is close to Ani_{max} if $K_T^\circ \gg \gamma/2\Phi$ and $1/\Phi$. If this requirement on K_T° is not fulfilled, $(\Delta I/I_{\text{mean}})_{\text{max}}$ is always smaller than Ani_{max}. Ani_{max} is thus a good indicator of the anisotropy of the scattered intensity.

Ani_{max} increases with γ/Φ, which reflects here the size of the nanoparticles. Working at constant γ/Φ, it varies with the ionic strength via $[\text{citrate}]_{\text{free}}$, which controls the interparticle interactions, and thus the osmotic pressure, Π.

At low Π (high $[\text{citrate}]_{\text{free}}$), if γ/Φ is not too small (here ≥ 7, i.e., $\lambda^* \geq 0.29$), then γ/Φ is close to K_T° or larger, so that Ani_{max} is large. It equals 2.1 for nanoparticle S7 at $[\text{citrate}] = 0.08$ mol/L. In this case, an anisotropy pattern is observed at low q. As Π is increased up to the top of the fluid phase region ($[\text{citrate}]_{\text{free}}$ is decreased), this anisotropy of scattered intensity progressively decreases and is directly given by Ani_{max}. Typically, here no anisotropy of scattered intensity can be detected under large applied fields for samples of $\text{Ani}_{\text{max}} \sim 0.1$ (nanoparticle S3); however, it is still possible for $\text{Ani}_{\text{max}} \geq 0.35$ (nanoparticle S7). Above a threshold of the pressure, the system

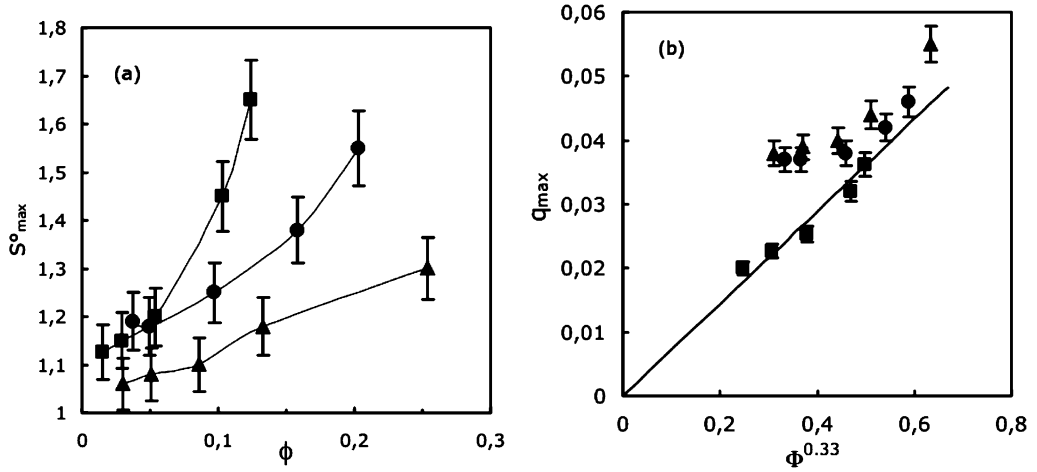

Figure 7. (a) Values of the maximum of the structure factor, S°_{max}, as a function of the volume fraction of the dispersions. The data are plotted for nanoparticle S7 and three $[citrate]_{free}$ concentrations: 0.003 M (squares), 0.03 M (circles), and 0.08 M (triangles). (b) Values of the abscissa q_{max} Å^{-1} of the peak of the structure factor for nanoparticle S7 as a function of $\Phi^{0.33}$. The symbols are the same as those in part a. The full line corresponds to the values of $q_{max} = 2\pi/d_{mean\ theor}$.

becomes solid with an amorphous structure.[30] In this region, Ani_{max} is small for our samples due to the strong interparticle repulsions. Therefore, as in the fluid phases of high pressures, the anisotropy of the patterns is small (nanoparticle S7) or not detectable (nanoparticle S3).

We conclude that this reduced parameter $Ani_{max} = (\gamma/\Phi)/K^{\circ}_{T}$ is a good reference tool to evaluate a priori the anisotropy that can be expected for a dispersion under a magnetic field for the patterns measured by scattering techniques at low q. It means that, although the anisotropy of compressibility depends on γ/Φ only, the observation of anisotropic scattered intensities is controlled by the position of the sample in the phase diagram, because it tunes K°_{T}.

V. Analysis of the Anisotropy of Structure at the Maximum of $S(q)$

Figures 1 and 4 show that there is an anisotropy of the structure factor on the scale of the wave vector q_{max} associated to the maximum of the structure factor, $S(q_{max}) = S_{max}$.

In zero field, the maximum value of the structure factor, S°_{max}, depends on the sample features Φ, $[citrate]_{free}$, and γ/Φ, as shown in Figure 7a for sample S7 ($\gamma/\Phi = 35$). For a given ionic strength, the dispersions are more and more structured, while Φ increases. For a given volume fraction, the dispersions are more structured, while the ionic strength decreases because the interparticle repulsion increases. The position of this maximum moreover corresponds to the most probable interparticle distance, defined as $2\pi/q_{max}$. If the interparticle repulsion is strong enough, the particles are homogeneously dispersed, and this most probable distance equals the mean distance between particles $(\pi/(6\Phi))^{1/3}d_{particles}$.[30] Figure 7b presents q_{max} as a function of $\Phi^{1/3}$ for sample S7 at several ionic strengths. For the lowest citrate concentration, q_{max} is proportional to $\Phi^{1/3}$, in good agreement with $q_{max} = 2\pi(6\Phi/\pi)^{1/3}d_{particles}$, expected for homogeneously dispersed particles. It means that, in this case of high interparticle repulsion, the most probable distance is indeed the mean interparticle distance. However, if the repulsion is decreased, q_{max} increases up to an upper limit of $q = 2\pi/d_{particles}$ corresponding to the contact between nanoparticles. This limit is not reached in the present experiment.

Under a field, an anisotropy in the height, $S_{max}(H,\theta)$, of the peak appears (Figure 4), which cannot be described anymore by the low q model of section III.3. In the direction perpendicular to the field, the peak is sharper than in the direction parallel to the field, meaning that the most probable distance between particles is better defined perpendicular to the field than parallel to the field. It expresses that the anisotropy of interactions is felt on the scale of the most probable distance and, on that scale, the effective interparticle repulsion is stronger in the direction perpendicular to the field than in the field direction.

For dispersions based on nanoparticles S3 and S7, the experimental dependences of $S_{max}(H,\theta)$ are presented in Figure 8. At first order, in the fluid phase, $[S_{max}(H, 0°) - S_{max}(H, 90°)]/S^{\circ}_{max} = (S^{||}_{max} - S^{\perp}_{max})/S^{\circ}_{max}$ is independent of Φ at constant $[citrate]_{free}$ and γ/Φ (see the inset of Figure 8a). Approaching the glass transition where the system solidifies, $(S^{||}_{max} - S^{\perp}_{max})/S^{\circ}_{max}$ begins to decrease (result not shown). This may be related to the progressive arrest of the dynamics (rotation and translation) while increasing the volume fraction.[43,44] Figure 8a shows the field dependence of $(S^{||}_{max} - S^{\perp}_{max})/S^{\circ}_{max}$ for two different γ/Φ values and several $[citrate]_{free}$ values in the fluid phase. It clearly expresses that the interparticle interaction depends on the orientation of the particles with a field, that the influence of $[citrate]_{free}$ is weak, and that the influence of γ/Φ is strong. Indeed, on this scale of the interparticle distance, the anisotropy of S_{max} results from the anisotropy of the dipolar interaction so that

$$(S_{max}(H,\theta) - S^{\circ}_{max})/S^{\circ}_{max} \propto (\gamma/\Phi)(1 - 3\cos^2\theta)L^2(\xi)$$

In this expression, $(\gamma/\Phi)(1 - 3\cos^2\theta)$ comes from the interaction between two dipoles and $L^2(\xi)$ comes from the orientation in the field of these two dipoles, which depends on the field strength. Thus, $(S^{||}_{max} - S^{\perp}_{max})/S^{\circ}_{max} \propto (\gamma/\Phi)L^2(\xi)$, in good agreement with the experiments performed with nanoparticles S3 and S7 (see Figure 8a), with the coefficient of proportionality being of the order of 1.2×10^{-2}. Figure 8b compares the angular dependence of $(S_{max}(H,\theta) - S^{\circ}_{max})/S^{\circ}_{max}$ obtained experimentally for nanoparticle S7 at $H = 8200$ Oe with the following expression: $4 \times 10^{-3}(\gamma/\Phi)(1 - 3\cos^2\theta)$. The agreement is quite good. Note that $S_{max}(H,\theta) = S^{\circ}_{max}$ for $\theta = 56°$, with the vanishing of the dipolar interaction being expected for $\cos\theta = \sqrt{3}/3$, that is, for $\theta = 54.7°$.

According to these results, it can be concluded that, on the scale of the interparticle distance, the structure is better defined

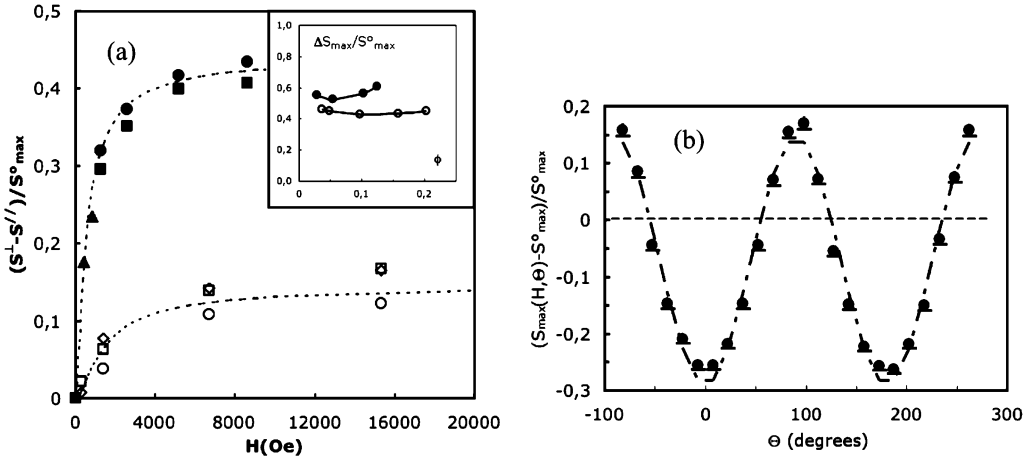

Figure 8. (a) $(S^{\perp} - S^{||})/S^{\circ}_{max}$ as a function of the magnetic field, H, for nanoparticles S3 and S7 for several values of Φ and $[citrate]_{free}$. S3 (open symbols): 7%, 0.0025 M (squares), 0.015 M (diamonds), 0.1 M (circles). S7 (full symbols): 3.7%, 0.03 M (squares), 9.7%, 0.03 M (circles), 13.3%, 0.08 M (triangles). The dashed lines are $(\gamma/\Phi)L^2(\xi)$, renormalized by the same constant of the order of 0.012 for S3 and S7. The inset plots $(S^{\perp} - S^{||})/S^{\circ}_{max}$ as a function of the volume fraction for two ionic strengths for nanoparticle S7. Full symbols, 0.003 M; open symbols, 0.03 M. (b) $(S_{max}(H,\theta) - S^{\circ}_{max})/S^{\circ}_{max}$ versus the angle, θ, between q and H. These data correspond to $H = 8200$ Oe $= 653$ kA/m, $[citrate]_{free} = 0.03$ M, and $\Phi = 9.7\%$ with nanoparticle S7. The line is $(1 - 3\cos^2\theta)$ normalized by 0.145.

in the direction perpendicular to the field with a higher repulsion in that direction. This balance of interactions is opposite to that obtained at low q, on large spatial scales. Similar experimental observations around q_{max} have been reported in ref 9 for a system of magnetic particles coated with silica, for which the interparticle interaction is strongly repulsive and the value of λ^* is low due to the silica shell. Therefore, as in our system, these nanoparticles are not able to form chains. Moreover, recent numerical simulations of our system, in the fluid region, present the same anisotropy of the peak:[41] the structure on the scale of the interparticle distance is less defined in the direction of the field.

VI. Conclusions

We have investigated by small angle neutron scattering (SANS) the influence of a magnetic field on the nanostructure of an aqueous magnetic fluid, the structure of which was already known in zero magnetic field. The dipolar interaction is varied in the range $7 < \gamma/\Phi < 34$ ($0.29 < \lambda^* < 1.42$). In this range, no chains are experimentally detected in these magnetic fluids, in good agreement with several simulations.[41,42] Thanks to the stabilization by an electrostatic repulsion, the ratio of isotropic over anisotropic interparticle interactions can be strongly varied by modifying the ionic strength in the solutions. Therefore, the magnetic fluids analyzed here are dispersions of individual nanoparticles. In the present study, we examine the fluid area of the phase diagram, thus the case of dominating interparticle repulsion. When a magnetic field, H, is applied, we moreover check experimentally that the dispersions remain monophasic with a global interaction that remains repulsive whatever the orientation with respect to H.

In the experiment, depending on the respective intensities of dipolar interaction and of repulsion, an anisotropy of the scattered intensity can be seen or not in the obtained patterns. It is observed, at low q, on large spatial scales, and in the region of the peak of the structure factor, on the scale of the interparticle distance.

The anisotropy of compressibility at low q is well described by the model of ref 10 whatever the parameters γ/Φ, H, and Φ and ionic strengths, that is, whatever the size of the particles and the interparticle interactions. On this large spatial scale, the dipolar interaction induces more repulsion in the direction parallel to the field than in the direction perpendicular to the field. On the contrary, on the scale of the peak of the structure factor, which corresponds to the interparticle distance, the structure is better defined in the direction perpendicular to the magnetic field.

Varying the dipolar interaction parameter through the nanoparticle size changes the anisotropy of the pattern both at low q and in the region of the peak of the structure factor. The anisotropy observed logically increases while increasing the ratio γ/Φ, allowing a *tuning of the amplitude of the magnetic field effect by varying the magnetic moment of the used nanoparticles.*

However, varying the isotropic interactions through the ionic strength changes the interparticle repulsion and the patterns of the scattered intensity in zero field. The ratio $Ani_{max} = (\gamma/\Phi)/K^{\circ}_{T}$, which quantifies the anisotropy of interactions, also roughly quantifies the anisotropy of the scattered intensities at low q and high magnetic field. It means that the anisotropy of the patterns depends on the location of the samples in the phase diagram (Figure 2), and that it is controlled by the balance of the isotropic interaction (K°_{T}) and of the dipolar interaction (γ/Φ). At low q and for given nanoparticles (γ/Φ fixed), this anisotropy is decreased while decreasing the ionic strength in the dispersions, that is to say, while increasing osmotic pressure. Consequently, the effects of the magnetic field may be observed, for example, in very repulsive fluids or amorphous solids (high osmotic pressures) only if the particles are large enough, which means that their dipolar moment is large (for example, for sample S7). However, for low osmotic pressures, the anisotropy of the scattered intensities is observed here whatever the dipolar moment (samples S3 and S7), which nevertheless controls the amplitude of this anisotropy.

Therefore, we conclude that (i) the anisotropy of compressibility is ruled by the parameter γ/Φ; (ii) *the anisotropy of the scattered intensity under a field is ruled for a large part by the structure without a field (K°_{T})*, which is controlled by the location of the sample in the plane of the phase diagram plotted in Figure 2. This is valid for all ferrofluids, whatever the nature of the stabilization, electrostatic or steric. The lack of control of the location of the samples in the phase diagram for a given volume fraction can lead, for example, to unreliable results under a magnetic field if phase separations are induced or to results difficult to compare from one sample to another. It may explain

the large discrepancies between the various experimental studies of the literature.

It would now be interesting with these ionic magnetic fluids to increase the role of the magnetic interaction either by decreasing interparticle repulsion or by directly increasing the magnetic dipolar interaction between nanoparticles.

Acknowledgment. We thank Delphine Talbot for the synthesis of samples S3 and S7.

References and Notes

(1) Rosensweig, R. *Ferrohydrodynamics*; Cambridge University Press: Cambridge, U.K., 1985.

(2) *Magnetic fluids and Applications Handbook*; Berkovski, Ed.; Begell House Inc. Publ.: New York, 1996.

(3) Holm, C.; Weis, J. J. *Curr. Opin. Colloid Interface Sci.* **2005**, *10*, 133−140.

(4) Pynn, R.; Hayter, J. B.; Charles, S. W. *Phys. Rev. Lett.* **1983**, *51* (8), 710−713.

(5) Anthore, R.; Petipas, C.; Chandesris, D.; Martinet, A. *J. Phys. (Paris)* **1977**, Colloq. 38, C2−C203. Anthore, R.; Gauthier, S.; Martinet, A.; Petipas, C.; *IEEE Trans. Magn.* **1980**, MAG-16, 197.

(6) Lal, J.; Abernathy, D.; Auvray, L.; Diat, O.; Grübel, G. *Eur. Phys. J. E* **2001**, *4* (3), 263.

(7) Pop, L. M.; Odenbach, S.; Wiedenmann, A.; Matoussevitch, N.; Bönnemann, H. *J. Magn. Magn. Mater.* **2005**, *289*, 303−306.

(8) Wiedenmann, A.; Hoell, A.; Kammel, M.; Boesecke, P. *Phys. Rev. E* **2003**, *68*, 031203-1−10.

(9) Autenrieth, T.; Wagner, J.; Hempelmann, R.; Härtl, W.; Robert, A.; Grübel, G. *Appl. Organomet. Chem.* **2004**, *18*, 520−522.

(10) Gazeau, F.; Dubois, E.; Bacri, J. C.; Boué, F.; Cebers, A.; Perzynski, R. *Phys. Rev. E* **2002**, *65*, 031403-1−15.

(11) Klokkenburg, M.; Vonk, C.; Claesson, E.; Meeldijk, J. D.; Erné, B. H.; Philipse, A. P. *J. Am. Chem. Soc.* **2004**, *126* (51), 16706−16707.

(12) Butter, K.; Bomans, P. H. H.; Frederik, P. M.; Vroege, J.; Philipse, A. P. *Nat. Mater.* **2003**, *2*, 88−91.

(13) Pshenichnikov, A. F.; Fedorenko, A. A. *J. Magn. Magn. Mater.* **2005**, *292*, 332−344.

(14) Shen, L.; Stachowiak, A.; Fateen, S.-E. K.; Laibinis, P. E.; Hatton, T. A.; *Langmuir* **2001**, *17*, 288−299.

(15) Aksenov, V. L.; Avdeev, M. V.; Balasoiu, M.; Bica, D.; Rosta, L.; Török, Gy.; Vekas, L. *J. Magn. Magn. Mater.* **2003**, *258*−*259*, 452−455.

(16) Itri, R.; Depeyrot, J.; Tourinho, F. A.; Sousa, M. H. *Eur. Phys. J. E* **2001**, *4* (2), 201−208.

(17) Büscher, K.; Helm, C.; Gross, C.; Glöckl, G.; Romanus, E.; Weitschies, W. *Langmuir* **2004**, *20*, 2435−2444.

(18) Klapp, S. H. L. *J. Phys.: Condens. Matter* **2005**, *17* (15), R525−R550.

(19) *Electrorheological Fluids, Magnetorheological Suspensions and Their Application*; Nakano, M., Koyama, K., Ed.; World Scientific Publishing Company: 1999. *Electrorheological Fluids and Magnetorheological Suspensions*; Bossis, G., Ed.; World Scientific Publishing Company: 2002.

(20) Pelster, R.; Spanoudaki, A.; Kruse, T. *J. Phys. D: Appl. Phys.* **2004**, *37*, 307−317.

(21) Hayes, C. F. *J. Colloid Interface Sci.* **1975**, *52*, 239.

(22) Bacri, J. C.; Salin, D. *J. Phys. Lett.* **1982**, *43*, L649.

(23) Bacri, J. C.; Perzynski, R.; Salin, D.; Cabuil, V.; Massart, R. *J. Magn. Magn. Mater.* **1990**, *85*, 27−32.

(24) Massart, R.; Dubois, E.; Cabuil, V.; Hasmonay, E. *J. Magn. Magn. Mater.* **1995**, *149*, 1−5.

(25) Kopcansky, P.; Tomco, L.; Marton, K.; Koneracka, M.; Potocova, I.; Timko, M.; Jadzyn, J.; Czechowski, G. *Phys. Status Solidi B* **2003**, *236* (2), 454−457.

(26) Pshenichnikov, A. F.; Shurubor, I. Yu. *Isv. Akad. Nauk, Ser. Fiz.* **1987**, *51*, 1081.

(27) Rosensweig, R. E.; Popplewell, J. *Int. J. Appl. Electromagn. Mater.* **1992**, 2 Suppl., 83.

(28) Jeyadevan, B.; Nakatani, I. *J. Magn. Magn. Mater.* **1999**, *201*, 62−65.

(29) Bacri, J. C.; Cebers, A. O.; Perzynski, R. *Phys. Rev. Lett.* **1994**, *72*, 2705−2708.

(30) Cousin, F.; Dubois, E.; Cabuil, V. *Phys. Rev. E* **2003**, *68*, 021405-1−9.

(31) Dubois, E.; Boué, F.; Cabuil, V.; Perzynski, R. *J. Chem Phys.* **1999**, *111* (15), 7147.

(32) Massart, R. *IEEE. Trans. Magn.* **1981**, *17*, 1247.

(33) Cousin, F.; Cabuil, V. *J. Mol. Liq.* **1999**, *83*, 203−215.

(34) Parsegian, V. A.; Fuller, N.; Rand, R. P. *Proc. Natl. Acad. Sci.* **1979**, *76* (6), 2750.

(35) Charlot, G. In *Les méthodes de la chimie analytique*; Masson et Cie, Ed., Masson: Paris, 1966, p 737.

(36) Gazeau, F.; Boué, F.; Dubois, E.; Perzynski, R. *J. Phys.: Condens. Matter* **2003**, *15* (15), S1305−S1334.

(37) Blums, E.; Cebers, A.; Maiorov, M. M. In *Magnetic Fluids*; de Gruyter: New York, 1997.

(38) Bacri, J. C.; Cebers, A.; Bourdon, A.; Demouchy, G.; Heegaard,; Kashevsky, B.; Perzynski, R. *Phys. Rev. E* **1995**, *52*, 3936.

(39) Kittel, C. *Introduction to Solid State Physics*, 7th ed.; John Wiley and Sons: New York, 1995.

(40) Mériguet, G.; Jardat, M.; Turq, P. *J. Chem. Phys.* **2005**, *123*, 144915.

(41) Mériguet, G.; Jardat, M.; Turq, P. *J. Chem. Phys.* **2004**, *121* (12), 6078−6085.

(42) Huang, J. P.; Wang, Z. W.; Holm, C. *Phys. Rev. E* **2005**, *71*, 061203.

(43) Mériguet, G.; Dubois, E.; Dupuis, V.; Perzynski, R. *In the 3rd International Symposium on Slow Dynamics in Complex Systems 2003*; Tokuyama, M., Oppenheim, I., Eds.; American Institute of Physics: Melville, NY; American Institute of Physics Conference Proceedings Vol. 708, 124−125, 2004.

(44) Mériguet, G.; Dubois, E.; Dupuis, V.; Perzynski, R. Forthcoming publication.